Laser-induced radiation leakage from microdroplets

Gang Chen, Dipakbin Q. Chowdhury, and Richard K. Chang

Department of Applied Physics and Center for Laser Diagnostics, Yale University, New Haven, Connecticut 06520-2157

Wen-Feng Hsieh

Institute of Electro-Optical Engineering, National Chiao-Tung University, Hsinchu, Taiwan

Received June 22, 1992; revised manuscript received November 10, 1992

Intensity distributions on the droplet surface and within the droplet are calculated and found helpful in explaining the observed laser-induced radiation leakage from various locations on or within the droplet. In an attempt to distinguish various possible mechanisms for laser-induced perturbation of micrometer-sized droplets, two types of experiment are conducted, and the measured intensity distribution is compared with that predicted by theoretical computation. The observed extra-light leakage of dye-laser radiation trapped in the droplet can be grouped into quasi-instantaneous and cumulative effects. One set of experiments uses a variable number of 100-ps laser pulses because of the laser's low fluence at 0.1 GW/cm^2. Quasi-instantaneous perturbations associated with an intensity-dependent index of refraction change are found to be important. Cumulative perturbations become evident as the number of 100-ps pulses increases. The second set of experiments uses one green laser beam and one near-IR laser beam, both with 7-ns duration, which because of the high fluence emphasize the electrostrictive- and temperature-related perturbations. Extra leakage from surface perturbations caused by the laser-induced temperature rise cannot be isolated but is found not to be dominant.

INTRODUCTION

The morphology-dependent resonances[1] (MDR's) of a transparent spherical droplet have small amounts of light leakage and thus have high values for the quality factor (Q) that provides gain enhancement and feedback for lasing,[2] stimulated Raman scattering[3] (SRS), and stimulated Brillouin scattering[4] (SBS). The lifetime τ of the internally generated radiation, which has a frequency, ω, near or on a MDR, is equal to Q/ω. The experimentally measured lifetime of the SRS generated within the droplet is in the nanosecond range,[5] corresponding to a $Q \approx 10^6$. We can envisage the internal radiation that is on a MDR as waves circulating within the droplet rim and leaking tangentially from the droplet rim. Any inhomogeneous perturbations in the volume refractive index or surface shape of an ideal sphere lower the Q value from that predicted by the Lorenz–Mie calculation.[1] Among the possible perturbations are thermally induced surface ripples,[6] unavoidable amounts of optical absorption, elastic scattering by internal gas bubbles,[7] and intensity depletion resulting from generation of other nonlinear waves.[5] Laser-induced perturbations, such as electrostrictive- and temperature-related surface bulge, intensity-dependent index-of-refraction change $\Delta m(\omega, I_{in})$, thermally induced index-of-refraction change $\Delta m(\omega, \Delta T)$, and density-dependent index-of-refraction change $\Delta m(\omega, \Delta\rho)$, can cause additional radiation leakage and can thereby further lower the MDR Q. In this paper we attempt to distinguish the various possible perturbation mechanisms that cause laser-induced radiation leakage from the droplet surface and interior.

Ray optics and Lorenz–Mie calculations of the internal and surface intensity distributions have shown that some of the input rays of a parallel plane wave, after refraction by the spherical illuminated face, converge toward a ring on the droplet shadow face. This ring of high surface intensity is referred to as the Descartes ring.[8–12] In addition, there exist two internal regions of high intensity just within the shadow face and the illuminated face where rays converge. These high-intensity regions can also cause laser-induced perturbation through above-mentioned mechanisms.

When viewed from the near-forward direction, red SRS leaking from the Descartes ring was reported when the water droplet, with radius $a = 60$ μm, was irradiated by a green laser beam with 10-ns pulse duration and $\lambda_{input} = 0.532$ μm.[8] The observation of laser-induced SRS leakage from the Descartes ring is significant because the extra emergence of SRS (other than tangentially from the rim of a perfect spherical droplet) has never been accounted for in the standard treatment of radiation leakage of nonlinear waves that is on a MDR. Consequently, questions arise as to the difference, if any, between the characteristics of SRS (or any other internally generated nonlinear radiation) from the Descartes ring and from the usual droplet rim. In addition, questions arise as to the laser-induced perturbation mechanism or mechanisms that cause the internally generated radiation that is on MDR's to leak and scatter from the surface and perturbed interior regions of maximum intensities. One form of surface perturbation is caused by laser-induced electrostrictive forces. Report[13] is made of the experimentally observed laser-induced electrostrictive bulging

0740-3224/93/040620-13$05.00

from the shadow face of a transparent droplet with a long-pulse (400-ns duration) and high-fluence (300 J/cm^2) laser beam. Calculations[14] have reproduced well the time evolution of the bulge amplitude and droplet shape.

The initial experimental observations of red SRS emerging from the Descartes ring and calculations of the surface intensity at the Descartes ring[8] have motivated several recent experiments with liquid droplets[9,10] and cylindrical jets.[11] These experiments on droplets and liquid columns provided the following facts: (1) the separately measured SRS characteristics from a portion of the Descartes ring and from the droplet rim have the same spectra, input-laser intensity thresholds, and delay times[9]; (2) the SRS intensity from the Descartes ring is higher than that from the droplet rim[9]; (3) with increased absorptive dye concentration in the smaller droplets ($a \approx 31$ μm), the SRS from the Descartes ring and the droplet rim have the same intensity threshold[9]; (4) with increased concentration of an absorptive dye in large droplets ($a \approx 64$ μm), the SRS from the Descartes ring has a higher threshold than that from the droplet rim[9]; (5) the SRS behavior from one of the two Descartes lines on the surface of a cylindrical liquid jet is similar to that from the Descartes ring on the surface of a droplet[11]; (6) the Descartes ring angle and the Descartes ring radius shrink with increasing refractive index[10]; and (7) the laser-induced radiation leakage has a prompt component and a persistent component.[10] For the prompt component the conjectured mechanisms are laser-induced nonlinear refractive-index gradient and plasma-related scattering effects. For the persistent component the conjectured mechanism is the laser-induced electrostrictive surface bulge.[10]

In this paper we present experimental and computational results that confirm and further the understanding of laser-induced perturbation mechanisms that can cause radiation leakage that emerges from regions of input-laser intensity maxima on the droplet surface and inside the droplet. We use two types of laser pulse in order to distinguish the quasi-instantaneous perturbations from the cumulative perturbations. To probe the quasi-instantaneous perturbation effects, one single 100-ps laser pulse is used. Multiple 100-ps pulses are used to probe the cumulative perturbation. In order to investigate and differentiate temperature-related effects from other possible laser-induced perturbation mechanisms, two laser beams of different color are used simultaneously. A green laser beam at 532 nm is absorbed by the dye-doped D_2O droplet, while there is no absorption of the near-IR laser beam at 1064 nm.

MECHANISMS FOR LIGHT LEAKAGE

The possible mechanisms for laser-induced radiation leakage from the Descartes ring on the droplet surface and from the localized regions within the droplet can be grouped into two categories. The first category is associated with elastic light scattering from the droplet surface and/or within the droplet as a result of inhomogeneous index of refraction induced by the following mechanisms: (1) the intensity-dependent index-of-refraction change [$\Delta m(\omega, I_{in}) = n_2 I_{in}(t)$] of droplets[9]; (2) the temperature-dependent index-of-refraction change [$\Delta m(\omega, \Delta T) = (\partial n/\partial T)\Delta T$, where ΔT is the laser-induced temperature rise]; (3) the index-of-refraction change caused by a local density change associated with the electrostrictive pressure and by the intense acoustic waves generated by the SBS field; and (4) the index-of-refraction change caused by the plasma that is generated after laser-induced breakdown (LIB) has been initiated.[10] The second category is associated with the following mechanisms that can cause surface bulging at the region of maximum surface intensity distribution: (1) the laser-induced electrostriction for a transparent droplet,[10,13,14] (2) the lowering of the surface tension because of an inhomogeneous temperature rise on the surface of an absorbing droplet, and (3) the localized acoustic waves generated by the SBS field.

The possible surface and volume perturbation mechanisms mentioned above can also be grouped according to their temporal responses, i.e., whether the perturbations are quasi-instantaneous or cumulative. Quasi-instantaneous perturbations are essentially dependent only on the instantaneous irradiance of the internal laser radiation and are not dependent on the history of the previous pulses. Quasi-instantaneous perturbations include the following mechanisms: intensity-dependent index-of-refraction change $\Delta m(\omega, I_{in})$; index-of-refraction changes caused by LIB-generated plasma; and index-of-refraction change associated with large wave-vector acoustic Brillouin phonons (with short lifetime) generated by the laser and the SBS fields. Cumulative perturbations are dependent on the time integral of the input-laser pulse fluence, i.e., the pulse energy. Such perturbations can continue to develop even after the laser pulse has ended. Cumulative perturbations include the following mechanisms: temperature-dependent index-of-refraction change $\Delta m(\omega, \Delta T)$; index-of-refraction change because of small wave-vector acoustic Brillouin phonons (with long lifetime)[15]; and surface bulge caused by laser-induced electrostriction, by lowering of the surface tension with an

Table 1. Possible Mechanisms for Light Emergence from a Descartes Ring

Categories	Possible Mechanisms	Characteristics
Index-of-refraction change	Intensity-dependent index of refraction: $\Delta m(\omega, I_{in}) = n_2 I_{in}(t)$	Quasi-instantaneous
	Temperature-dependent index of refraction: $\Delta m(\omega, \Delta T) = (\partial n/\partial T)\Delta T$	Cumulative
	Acoustic Brillouin phonons: $q > k_L$	Quasi-instantaneous
	Acoustic Brillouin phonons: $q \ll k_L$	Cumulative
	Plasma	Quasi-instantaneous
Surface bulge	Electrostriction	Cumulative
	Temperature lowering of surface tension	Cumulative
	Acoustic Brillouin phonons: $q > k_L$	Quasi-instantaneous
	Acoustic Brillouin phonons: $q \ll k_L$	Cumulative

inhomogeneous temperature rise on an absorbing droplet surface, and by acoustic waves generated by the nonlinear beating of the SBS and laser waves. The acoustic phonons with small wave vector q (compared to the wave vector of light k_L) have a long lifetime and thus can lead to a cumulative effect.[15] Conversely, the acoustic phonons with $q > k_L$ have short lifetime and thus are quasi-instantaneous. The various laser-induced perturbations are summarized in Table 1.

Typical values for parameters associated with the above-mentioned laser-induced perturbation are $n_2 = 514 \times 10^{-16}$ cm^2/W and $\partial n/\partial T = -8 \times 10^{-4}$/deg C for CS_2, and $n_2 = 7.6 \times 10^{-16}$ cm^2/W and $\partial n/\partial T = -4 \times 10^{-4}$/deg C for ethanol. The temperature rise ΔT associated with a laser pulse with fluence $I\Delta t$ is $\Delta T = I\Delta t\alpha/(C_p\rho)$, where I is the local input-laser intensity, Δt is the full width at half maximum of the incident pulse, α is the absorption coefficient, C_p is the specific heat ($C_p = 1.00$ J/deg M for CS_2 and $C_p = 2.44$ J/deg M for ethanol), and ρ is the density of the liquid ($\rho = 1.26$ gm/cm^3 for CS_2 and $\rho = 0.79$ gm/cm^3 for ethanol).

COMPUTED SURFACE AND INTERNAL INTENSITY DISTRIBUTIONS

Ethanol Droplets

The surface and internal intensity distribution are well understood by using ray optics[12] and Lorenz–Mie formalisms.[13] Both approaches have shown that the incident laser intensity has a relative maximum at the Descartes ring on the droplet surface. Figure 1(a) shows the intensity distribution at the equatorial plane of the droplet calculated with Lorenz–Mie theory for an ethanol droplet in air with radius $a = 35.4$ μm, index of refraction $m(\omega) = 1.36$, and input laser wavelength $\lambda_{input} = 0.532$ μm. Intensity is defined as $E \cdot E^*$, where E is the electric field. We assume the incident beam to be a plane wave propagating along the droplet diameter or the y axis, and the λ_{input} is not on an input MDR. The internal intensity plot along the y axis [see Fig. 1(b)] shows that the internal intensity reaches an absolute maximum (400 times larger than the incident light intensity) in a small region along the droplet principal diameter ($x = 0$) and just within the droplet shadow surface (near $y/a = 1$), known as front-focal spot. Also, there is a second high-intensity region located at the droplet principal diameter and just within the droplet illuminated surface (near $y/a = -1$), known as back-focal spot. From ray optics these internal intensity maxima are formed by rays that are reflected from the droplet surface and intersect at the high-intensity regions. When the droplet is irradiated with a plane wave, nonlinear interactions take place mainly at this front-focal spot because this internal region has the highest intensity. The third internal high-intensity region occurs as a cone, where the rays converge toward the droplet shadow face [see Fig. 1(a)].

The surface intensity toward the shadow side of the equator is shown in Fig. 1(c). The vertical axis is the relative intensity with respect to the incident beam intensity, and the horizontal axis is the polar angle ϕ, where $\phi = 0°$ is along the positive y axis in Fig. 1(a). The surface intensity maximum is not at the principal diameter ($x = 0$, $y/a = 1$) but is located at $\phi \approx 18°$, which coincides with the Descartes angle[8] ϕ_D. The Descartes angle is de-

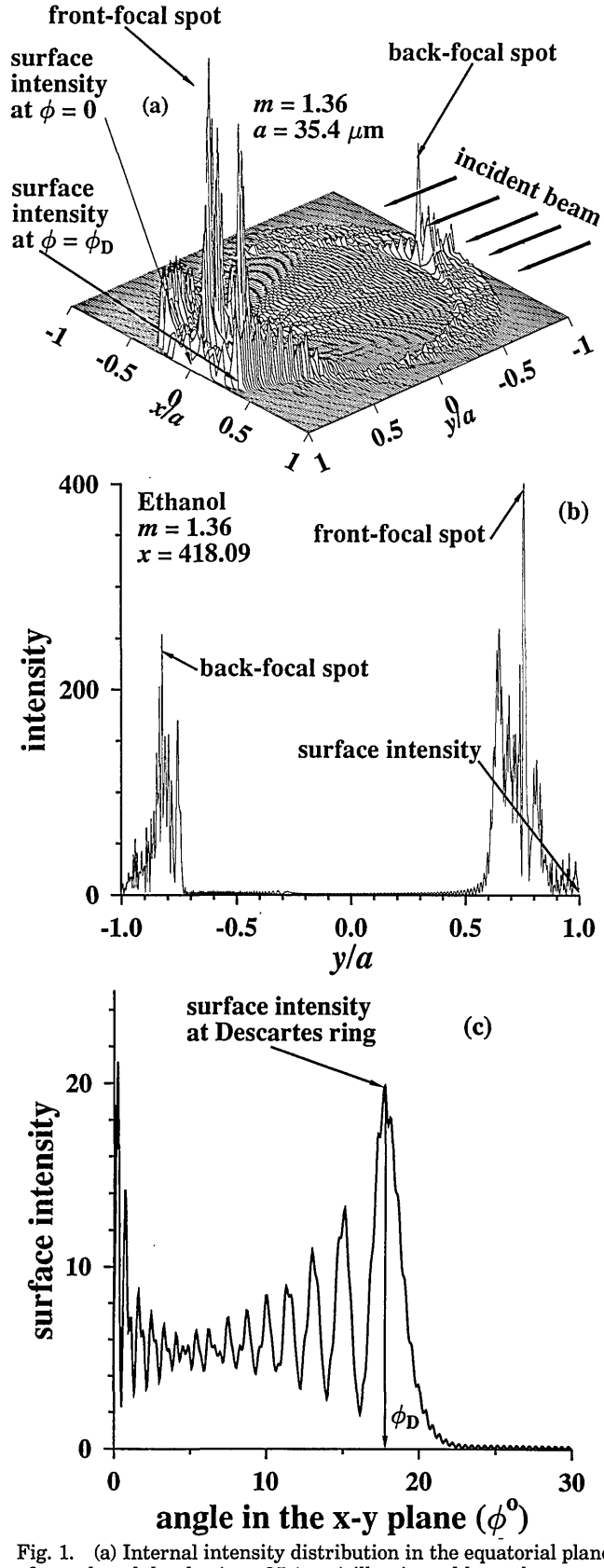

Fig. 1. (a) Internal intensity distribution in the equatorial plane of an ethanol droplet ($a = 35.4$ μm) illuminated by a plane wave with $\lambda_{input} = 0.532$ μm. (b) The intensity distribution along the principal diameter (y axis) of the droplet. (c) The intensity distribution along the shadow surface of the equatorial plane (x–y plane) as a function of the angle ϕ from the principal diameter (y axis). The incident laser polarization is normal to the equatorial plane and $m(\omega) = 1.36$. Because of lower spatial resolution, (a) does not show all the details shown in (b) or (c).

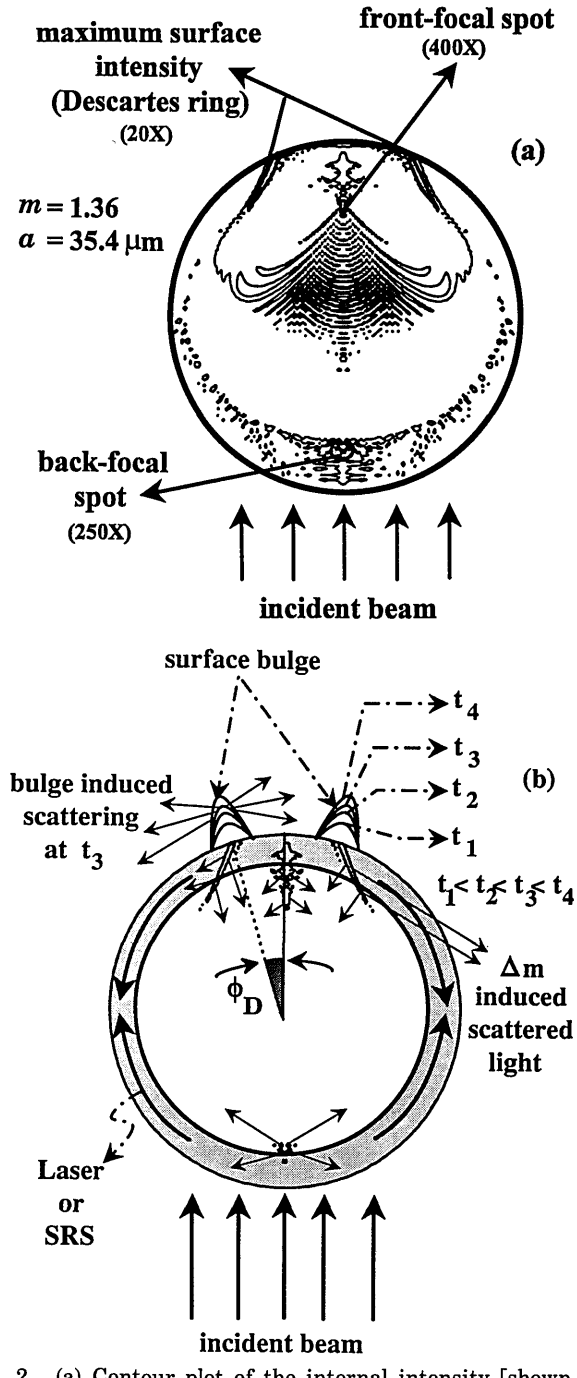

Fig. 2. (a) Contour plot of the internal intensity [shown in Fig. 1(a)] for the same ethanol droplet. The locations of the front-focal spot, the back-focal spot, and the maximum surface intensity (located at the Descartes angle ϕ_D) are shown. (b) The spatial distribution of the lasing or SRS field that is on MDR's is superimposed upon the intensity contour plot. Possible locations are illustrated for extra elastic leakage because of surface bulge that is developing in time and for extra scatterings because of internal index-of-refraction perturbation [$\Delta m(\omega)$]. The amplitude of the surface bulges at $\phi = \phi_D$ is greatly exaggerated.

fined (according to ray optics) as the largest angle from the droplet x axis on which the rays from the illuminated face converge. From ray optics calculation, $\phi_D = 180° - 2\sin^{-1}\{[4m^2(\omega) - 4]/3m^2(\omega)\}^{1/2} - \sin^{-1}\{[4 - m^2(\omega)]/3\}^{1/2}$. Since the droplet has rotational symmetry about the principal diameter (y axis) for a circularly polarized incident plane wave, the surface intensity maximum is a ring on the droplet shadow face that is named the Descartes ring. The intensity enhancement at the Descartes ring is approximately 20× [see Fig. 1(c)], which is still an order of magnitude smaller than the 400× intensity enhancement at the front-focal spot [see Fig. 1(b)]. The surface intensity peak at ϕ slightly larger than 0° is also enhanced by approximately 20×, but the area under that peak is much smaller compared with the area under the peak at ϕ_D [see Fig. 1(c)].

Figure 2(a) shows the contour plot of the internal intensity for the same droplet parameters as those used in calculating the intensity distribution shown in Fig. 1. In Fig. 2(a) the laser beam is propagating from the bottom toward the top, and the shaded areas indicate the front-focal spot, the back-focal spot, the Descartes ring, and the cone region just before the Descartes ring. Some possible perturbation mechanisms that can cause radiation leakage are shown in Fig. 2(b). Because MDR's provide feedback for lasing or SRS in the droplet, the lasing and SRS radiation adopt the internal field distribution of the MDR's and can be envisaged as two counterpropagating waves confined within the droplet rim (see the shaded ring). The appropriate MDR's must have some spatial overlap with the front-focal spot, because it is the high intensity at the front-focal spot that provides the pumping for the lasing or SRS process.

Inside the droplet, the high-intensity regions of the front- and back-focal spots as well as the cone region can induce index of refraction changes $\Delta m(\omega)$ associated with $n_2 I_{in}(t)$ and $(\partial n/\partial T)\Delta T$. The straight arrows in Fig. 2(b) denote the possible extra elastic scattering from various regions where $\Delta m(\omega)$ may be induced. On the droplet surface, the high-intensity region at the Descartes angle can induce $\Delta m(\omega)$ and hence some emergence of extra elastic scattering at the Descartes ring. Surface bulge will also cause extra leakage of the lasing or SRS waves that are on MDR's. Electrostrictive force and temperature-related surface tension lowering can cause surface distortions that develop long after the input-laser pulse has ended. For small-amplitude bulge and $\Delta m(\omega)$ the radiation that is leaking at the Descartes ring should emerge tangentially to the droplet surface. As the bulge amplitude continues to grow [shown exaggeratedly in Fig. 2(b) for different times], more light should progressively leak out at the surface bulge.

CS_2–Ethanol Droplets

Figure 3(a) shows the computed equatorial intensity distribution, Fig. 3(b) shows the axial intensity, and Fig. 3(c) shows the surface intensity near the shadow face for a CS_2–ethanol (with 80% CS_2 and 20% ethanol) droplet of $a = 25.5$ μm. The CS_2–ethanol droplet has $m(\omega) = 1.54$, and the incident laser wavelength is 0.532 μm. Note that the internal intensity distribution is changed when $m(\omega)$ is increased from 1.36 to 1.54 [compare Figs. 1(a) and 1(b) with Figs. 3(a) and 3(b)]. The intensity enhancement at the front-focal spot of a droplet with $m(\omega) = 1.54$ has increased slightly relative to that with $m(\omega) = 1.36$, for example, an intensity maximum of ≈450× in Fig. 3(b) versus that of ≈400× in Fig. 1(b). The intensity in the internal region along the principal axis between the droplet shadow surface and the front-focal spot for a CS_2–ethanol droplet has increased (on average) by approxi-

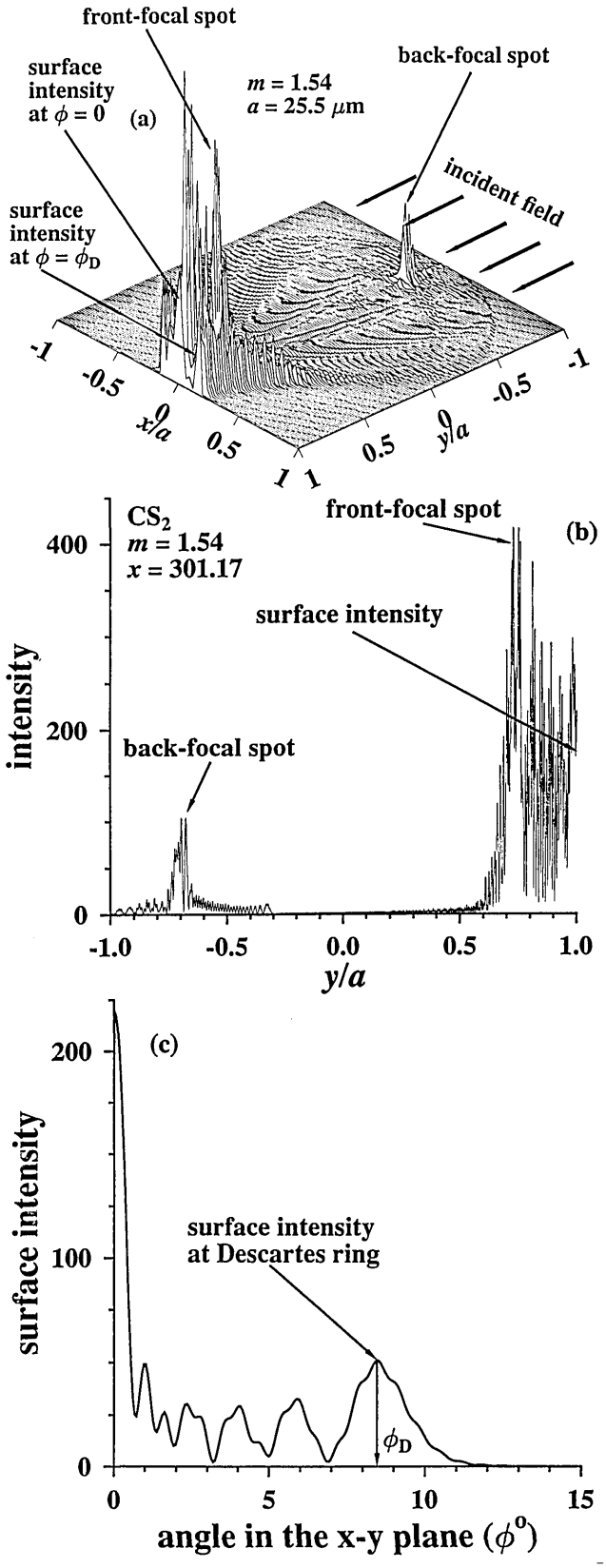

Fig. 3. (a) Internal intensity distribution in the equatorial plane of a CS_2–ethanol (80% CS_2 and 20% ethanol) droplet (a = 25.5 μm) illuminated by a plane wave with $\lambda_{input} = 0.532\ \mu m$. (b) The intensity distribution along the principal diameter of the droplet (y axis). (c) The intensity distribution along the shadow surface of the equatorial plane (x–y plane) as a function of the angle ϕ from the principal diameter (y axis). The incident laser polarization is normal to the equatorial plane, and $m(\omega) = 1.54$. Because of lower spatial resolution, (a) does not show all the details shown in (b) or (c).

mately 5× relative to that for an ethanol droplet [see Fig. 3(b)]. Figure 3(c) shows that although there is a local maximum in the surface intensity at $\phi_D = 8.6°$ for CS_2–ethanol droplets, the absolute maximum in the surface intensity is now shifted to $\phi = 0°$. In fact, the maximum surface intensity is approximately 240× larger than the input-laser intensity and approximately 5× larger than

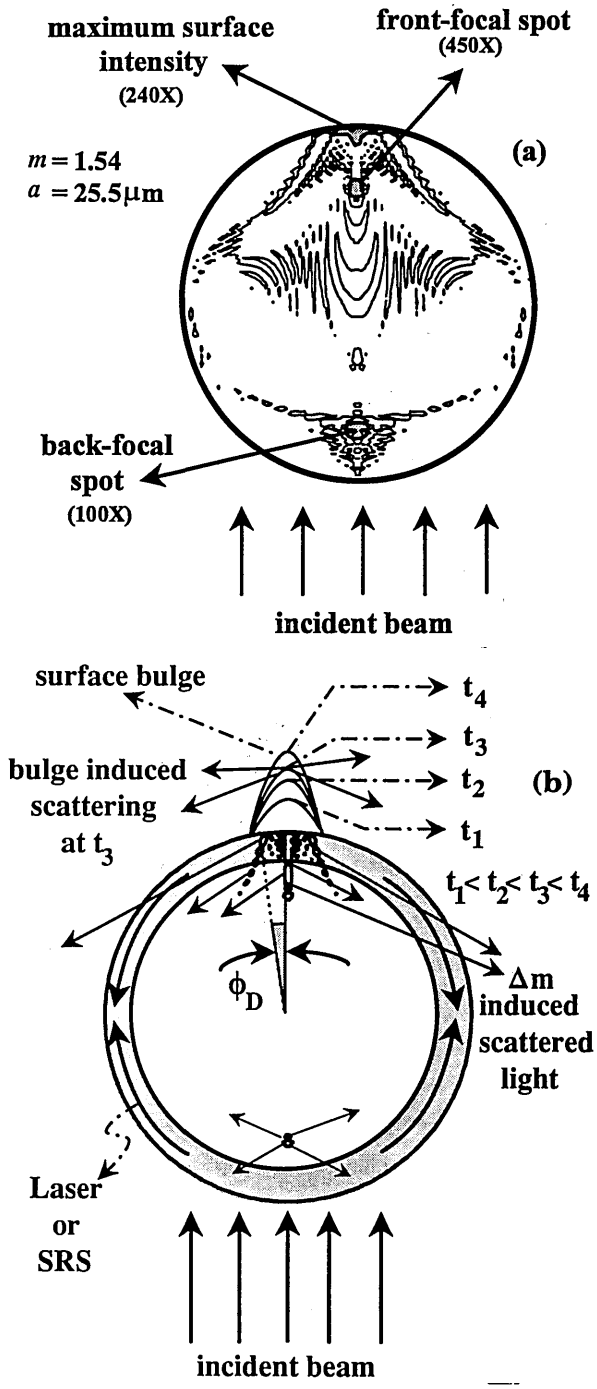

Fig. 4. (a) Contour plot of the internal intensity [shown in Fig. 3(a)] for the same CS_2–ethanol droplet. The locations of the front-focal spot, the back-focal spot, and the maximum surface intensity (located now at $\phi = 0°$ and not at the Descartes angle ϕ_D) are shown. (b) The spatial distribution of the lasing or SRS field that is on MDR's is superimposed upon the contour plot. Possible locations are illustrated for extra leakage because of surface bulge that is developing in time and for extra elastic scattering because of internal index of refraction perturbation [$\Delta m(\omega)$]. The amplitude of the surface bulges at $\phi = 0°$ is greatly exaggerated.

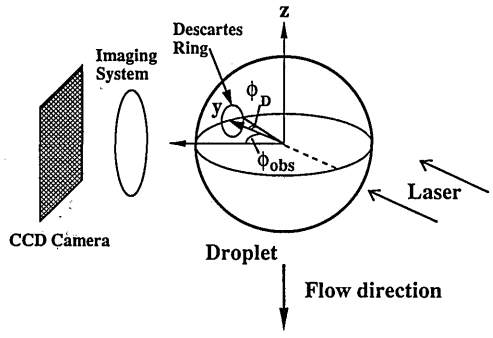

Fig. 5. Droplet flow direction and collection optics shown with respect to the incident laser direction (y axis) and the Descartes ring. The incident beam is propagating in the y direction and polarized in the z direction. The observation angle ϕ_{obs} is with respect to the y axis.

the surface intensity at ϕ_D. Also, this maximum surface intensity is approximately 10× larger than that at $\phi_D = 18°$ for the ethanol droplet with $m(\omega) = 1.36$.

Figure 4(a) shows the contour plot of the internal intensity for the CS_2–ethanol droplet. The shaded areas indicate high-intensity regions located at the front-focal spot, the back-focal spot, and within the surface at $\phi = 0°$. Figure 4(b) exaggeratedly depicts the possible mechanisms of light emergence from high-intensity regions on the droplet surface and within the droplet. Because the highest surface intensity is now located at $\phi = 0°$, any laser-induced perturbations [surface bulge and/or $\Delta m(\omega)$] will be dominated by the surface intensity maximum at $\phi = 0°$ rather than at the Descartes ring ($\phi_D = 8.6°$). Figure 4(b) shows the surface bulge amplitude at $\phi = 0°$ to be growing in time. In principle, the extra leakage from the surface (at $\phi = 0°$ and $\phi_D = 8.6°$) and the interior (at the front-focal spot) should be spatially distinguishable. Internally to the droplet, any inhomogeneous $\Delta m(\omega)$ will cause elastic scattering of the lasing or SRS waves that are circulating around the droplet rim (see the solid-line arrows).

EXPERIMENTAL DETAILS

Equipment Setup

A modified Berglund–Liu vibrating orifice droplet generator produces a linear stream of monodispersed droplets. Figure 5 shows that the droplets are flowing along the vertical z axis at approximately 5 m/s. A two-dimensional CCD camera is placed along the horizontal axis and digitally photographs the radiation leaking from various portions of the droplet. The angle ϕ between the incident laser beam direction (defined to be along the droplet y axis) and the collection-optics axis is approximately 38°. The Descartes ring has an angle ϕ_D with respect to the incident laser beam direction (y axis). The polarization of the input beam is vertical relative to the horizontal scattering plane shown in Fig. 5. The laser beam radius is slightly larger than the droplet radius, and thus the plane wave assumed in the calculations of the internal intensity distribution (shown in Figs. 1 and 3) is valid.

A CCD camera is chosen to capture and digitize the image of the droplet because the CCD has a much larger dynamic range than photographic film. The digitized information enables us to measure quantitatively the leakage intensity from different portions of the droplet. For the lasing spectrum measurements the same CCD camera is placed at the exit plane of a spectrometer and simultaneously detects the spatially resolved droplet-lasing spectra.

The incident laser beam is from the green second-harmonic output ($\lambda = 0.532$ μm) of a cw-pumped Q-switched mode-locked Nd:YAG laser. Each Q-switched burst contains 17 mode-locked pulses. The irradiance of the most intense pulse in each Q-switched burst is ≈0.1 GW/cm^2. The duration of each mode-locked pulse is 100 ps, and the pulse-to-pulse separation is $t_{p-p} \approx 13.2$ ns. An electro-optic pulse selector is used to pass any desirable number of consecutive 100-ps pulses within each Q-switched burst. The pulse selector is synchronized with the laser Q switch and the frequency oscillator of the droplet generator. There are two main reasons for choosing the combination of mode-locked laser and pulse selector: (1) the irradiance of a single pulse is high enough to induce quasi-instantaneous perturbations, such as $\Delta m(\omega, I_{in}) = n_2 I_{in}(t)$, but at the same time its fluence is low enough to cause no appreciable cumulative effect; (2) this combination provides the ability to choose multiple pulses to investigate the cumulative perturbations. The temporal profile of the incident laser pulse is detected by a P-I-N photodiode, which is monitored by an oscilloscope. Figure 6 is a photograph of the oscilloscope screen.

We also used a flash-lamp-pumped Q-switched Nd:YAG laser in order to emphasize cumulative perturbations. This laser produces a single pulse with pulse duration of ≈7 ns, irradiance of ≈0.1 GW/cm^2, and fluence of ≈0.7 J/cm^2. There are two main reasons to use the 7-ns pulse to complement our measurements with a single 100-ps pulse: (1) the single 7-ns pulse has nearly the same irradiance as the 100-ps pulse but 70× more fluence; (2) the Q-switched Nd:YAG laser with the second-harmonic converter simultaneously emits in the green ($\lambda_{input} = 0.532$ μm) and in the near IR ($\lambda_{input} = 1.064$ μm). The fact that the green pulse is absorbed and the near-IR pulse is not is used to isolate the temperature-related perturbation effects from the other mechanisms.

Types of Liquid Droplets

In all our experiments we chose to monitor the leakage of laser radiation from droplets containing Rhodamine 6G dye and not the leakage of SRS radiation from pure liquid droplets. Since lasing has a much lower threshold than SRS, the incident laser irradiance can be lowered greatly to prevent the LIB threshold from being reached. Consequently, plasma-related perturbations can be neglected in our experiments, since the input intensity never exceeded

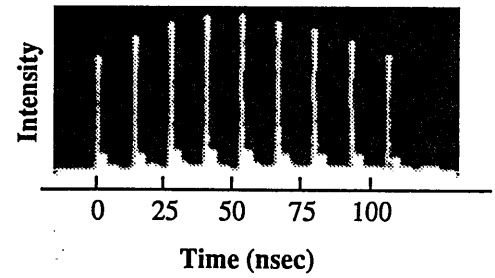

Fig. 6. Oscilloscope trace of the Pockels cell selected pulses from the second-harmonic output of a Q-switched mode-locked Nd:YAG laser. Each pulse has 100-ps duration and a pulse-to-pulse separation of $t_{p-p} = 13.2$ ns.

0.1 GW/cm^2 for both the 100-ps and the 7-ns pulses. The additional advantage in choosing laser-dye-doped droplets is the suppression of SBS generated by the green laser beam. At $\lambda_{input} = 0.532$ μm and with 2×10^{-4} M Rhodamine 6G dye, the absorption coefficient is $\alpha \approx 7$ cm^{-1}. Such large absorptivity greatly lowers the Q of the MDR at green, and hence SBS never reaches its threshold. In fact, we cannot even observe any SBS in a 10-cm-long optical cell when the Rhodamine 6G dye concentration is decreased to 2×10^{-6} M. In our droplet experiments, any possible laser-induced perturbations associated with acoustic Brillouin phonons can be neglected. However, by choosing to monitor the leakage of laser radiation instead of the SRS, we introduced absorption loss associated with the laser dye and hence inadvertently introduced complications as a result of temperature rise effects.

Ethanol droplets containing 2×10^{-4} M Rhodamine 6G are used to study the quasi-instantaneous and cumulative effects of laser-induced radiation leakage of laser radiation from various parts of the ethanol droplet. A binary mixture of CS_2 and ethanol droplets (80% CS_2 and 20% ethanol) also containing 2×10^{-4} M Rhodamine 6G is investigated in order to increase the $\Delta m(\omega, I_{in})$ perturbations. The estimated index of refraction for the binary mixture is $m(\omega) = 1.54$. The addition of CS_2 is chosen for several reasons. First, CS_2 has a larger $m(\omega)$ than ethanol [i.e., $m(\omega) = 1.63$ for CS_2 versus $m(\omega) = 1.36$ for ethanol], and, consequently, the surface intensity maximum moves to $\phi = 0°$ for the binary-mixture droplets used in our experiment. Second, the intensity-dependent index-of-refraction coefficient n_2 for CS_2 is $\approx 100\times$ larger than that for ethanol (i.e., $n_2 = 514 \times 10^{-16}$ cm^2/W for CS_2 and $n_2 = 7.6 \times 10^{-16}$ cm^2/W for ethanol). Consequently, the $\Delta m(\omega, I_{in})$ perturbation in the binary-mixture droplets should be considerably larger than that in pure ethanol droplets. Third, the electrostriction coefficient γ_e of CS_2 is only $\approx 2\times$ larger than that of ethanol since $\gamma_e = [m^2(\omega) - 1][m^2(\omega) + 2]/3$. Fourth, the surface tension σ of a CS_2–ethanol mixture is comparable with that of ethanol ($\sigma = 32.33$ dyne/cm for CS_2 and $\sigma = 24.05$ dyne/cm for ethanol). Finally, Rhodamine 6G dissolved in ethanol can remain dissolved in the binary mixture of CS_2 and ethanol. We noted that the lasing threshold for the binary mixture of CS_2 and ethanol is almost the same as that for pure ethanol. Again, because of the low-input irradiance of 0.1 GW/cm^2, we can neglect plasma-related perturbations, as no laser-induced breakdown occurs for the CS_2–ethanol droplets. In addition, because of the strong laser-dye absorption in the green ($\alpha = 7$ cm^{-1}), we can neglect the generation of SBS, which might induce acoustic phonon-related perturbations. However, as we discussed above, the strong absorption can cause temperature-related effects.

EXPERIMENTAL RESULTS AND DISCUSSIONS

One or More 100-ps Pulses: Ethanol Droplets

Figure 7(a) shows the CCD-captured image of a lasing ethanol droplet ($a = 35.4$ μm) irradiated with five consecutive 100-ps laser pulses (within a single Q-switched burst). The viewing angle with respect to the incident laser beam is $\phi_{obs} = 38°$. The outer red ring corresponds to the normal lasing radiation leaking of MDR's from the unperturbed droplet rim. The detected red crescent corresponds to the leaking of the dye-laser radiation that is on a MDR as a result of the laser-induced perturbations on the droplet surface at the Descartes ring.

Figure 7(b) is the digitized plot of the same CCD image shown in Fig. 7(a). The arrow points to the center Track A, which corresponds to the droplet equatorial plane shown in Fig. 7(c). The intensity peaks along Track A are labeled 1, 2, and 3 in Fig. 7(b). Figure 7(c) indicates the projection onto Track A the radiation leaking from droplet rim (peaks 1 and 3) and from one part of the Descartes ring.

The illustration shown in Fig. 8 is intended to clarify the origins of the lasing radiation leakage from the rim, which appears as a ring, and from the Descartes ring, which appears as a crescent. Figure 8 shows the top view of the droplet and the lasing waves that are counterpropagating within the droplet equatorial plane. Only fractions of the tangentially emerging MDR leakage rays from the rim in the x–y plane are within the acceptance angle of the imaging system and produce two red dots on the CCD Track A at points 1 and 3. Viewing at $\phi_{obs} = 38°$, we depict only rays 1 and 3, because these two rays have the highest intensity per unit ϕ angle or droplet arc length. In three dimensions the CCD image from corre-

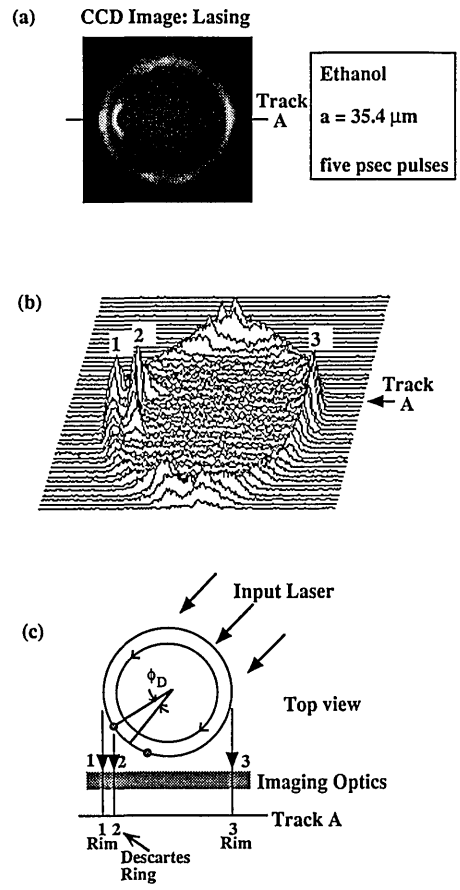

Fig. 7. (a) Gray-scale image from the CCD camera of an ethanol droplet (containing 2×10^{-4} M Rhodamine 6G) irradiated by five consecutive 100-ps green ($\lambda_{input} = 0.532$ μm) pulses within a single Q-switched burst. (b) The digitized CCD image shown in (a). (c) An illustration of the specific regions on the droplet equatorial plane that the leakage radiation is detected along CCD Track A.

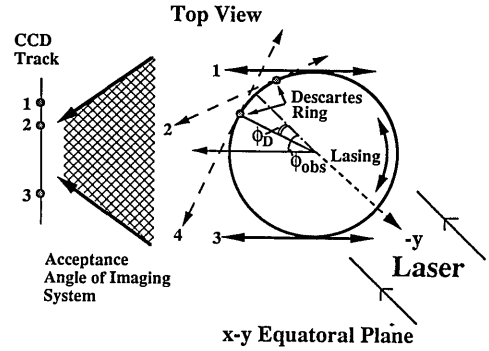

Fig. 8. Illustration (top view) of the lasing radiation that tangentially leaks from the droplet rim and the surface perturbation at the Descartes ring. Rays 1, 2, and 3 are within the acceptance angle of the collection lens and are imaged on the CCD detector.

sponding regions to points 1 and 3 should consist of a red ring exactly at the droplet rim. Figure 8 further shows that the tangentially emerging rays (labeled 2 and 4) are leaking from the Descartes ring center at $\phi = 38°$ relative to the principal diameter of the droplet (y axis). Because of the finite acceptance angle of collection optics, only ray 2, which emerges tangentially at the Descartes ring, appears on the CCD Track A as point 2 [see Fig. 7(c)]. Ray 4, which emerges tangentially from the opposite portion of the Descartes ring, is outside the acceptance angle of the imaging system. In three dimensions, all the rays corresponding to ray 2 in Fig. 8 produce a crescent, while all the rays corresponding to ray 4 are never collected by the imaging system. Our collection optics (with $\approx 50\times$ magnification) has a depth of field of less than 5 μm. Consequently, the droplet rim and the Descartes ring cannot both be in focus, because the Descartes ring is closer to the collection optics than the droplet rim is. The CCD image shown in Fig. 7(a) is captured with the collection optics adjusted so that the Descartes arc is in focus and the droplet rim is out of focus and therefore appears to be slightly blurred.

CCD images, similar to Figs. 7(a) and 7(b), are taken as a function of the number of consecutive 100-ps pulses that are separated by 13.2 ns. Figures 9(a), 9(b), and 9(c) show three digitized intensity plots of lasing ethanol droplets that are irradiated with one, two, and five 100-ps pulses, respectively. Although the overall detected intensity increases with the number of laser pulses, the relative intensities shown in Fig. 9 are normalized. For each digitized intensity plot the intensity distribution along Track A, which corresponds to laser radiation leaking from various portions on the droplet equatorial plane, is plotted as a thick line. Intensity peaks 1 and 3 correspond to light leaking from the droplet rim at the equatorial plane. Intensity peak 2 corresponds to light leaking from one part of the Descartes ring that intersects the equatorial plane.

Even when a single 100-ps pulse (with an irradiance of ≈ 0.1 GW/cm^2) irradiates the Rhodamine 6G-doped ethanol droplet, the existence of intensity peak 2 in Fig. 9(a) indicates that there is a dye-lasing radiation leakage from the Descartes ring. The presence of leakage at the Descartes ring with one 100-ps pulse is somewhat surprising. The electrostrictive impulse momentum imparted on the droplet surface by a single 100-ps laser pulse is small. In addition, the bulge amplitude does not have time to develop during the droplet cavity lifetime, which is approximately 10 ns. The electrostrictive bulge amplitude resulting from a single 100-ps pulse with fluence of ≈ 0.01 J/cm^2 and during the 10-ns photon lifetime can be estimated from the previous surface bulge amplitude photographs of H_2O droplets[13,14] (with $a = 50$ μm), which attained the maximum bulge amplitude of approximately 5 μm some 2 μs after a single 400-ns pulse with 300 J/cm^2. When we assume that the bulge amplitude is linearly proportional to the pulse fluence and the delay time after the input-laser pulse is off, the estimated bulge amplitude after 10 ns is of the order of angstroms. Consequently, the extra leakage at the Descartes ring because of electrostrictively induced surface bulge resulting from a single 100-ps pulse is negligible.

However, there can be other perturbations that are induced by a single 100-ps pulse. The $\Delta m(\omega, I_{in}) = n_2 I_{in}(t)$ perturbation depends only on the laser irradiance, which is enhanced by approximately 20× at the Descartes ring for ethanol droplets. We estimate that at the Descartes ring the quasi-instantaneous $\Delta m(\omega, I_{in}) \approx 1.5 \times 10^{-6}$. A single 100-ps pulse with ≈ 0.1-GW/cm^2 fluence can also in-

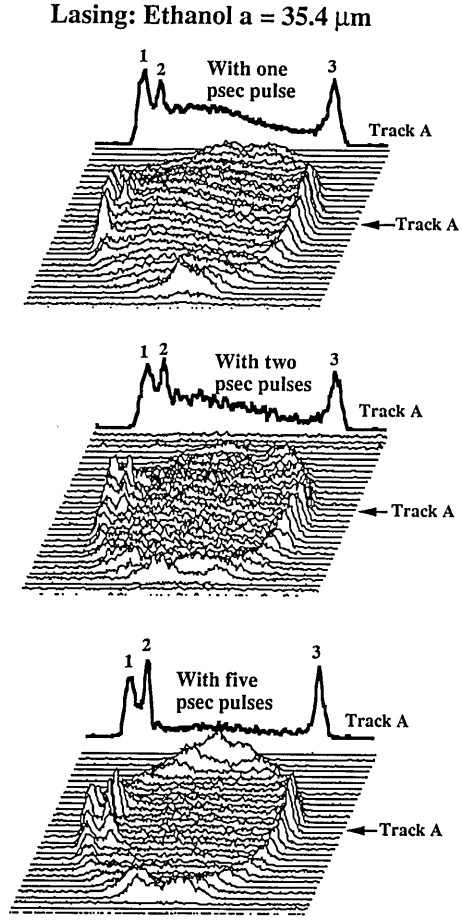

Fig. 9. Digitized CCD images of dye-laser leakage intensity for (a) one, (b) two, and (c) five 100-ps pulses with $t_{p-p} = 13.2$ ns illuminating the ethanol droplets containing 2×10^{-4} M Rhodamine 6G. On top of each digitized plot the content in CCD Track A (corresponding to the droplet equatorial plane shown in Fig. 8) is plotted with a thick line. Intensity peaks 1 and 3 are the normal MDR leakage from the droplet rim, and intensity peak 2 is the extra leakage from the surface bulge at the Descartes ring.

troduce small amounts of heat. Thus there are temperature-related perturbations at the droplet surface. The estimated surface temperature rise at the Descartes ring is $\Delta T \approx 0.7°$, which can give rise to a $\Delta m(\omega, \Delta T) \approx -3 \times 10^{-4}$ at the Descartes ring. We are unable to estimate reliably the surface bulge amplitude caused by the surface tension lowering that is due to a $\Delta T \approx 0.7°$ rise. Thus, based on the single 100-ps input-laser pulse result, the observation of light leakage from the Descartes ring cannot be ascribed uniquely to either quasi-instantaneous or cumulative perturbation.

Figure 9 shows that the intensity ratio of peak 2 and peak 1 increases when the number of 100-ps pulses is increased from one pulse to two pulses and then to five pulses. Because the radiation leaking from the droplet rim is just the normal MDR-related leakage, the leakage rate is independent of the existence of previous pulses. Consequently, the total detected rim intensity should scale linearly with the number of pulses, assuming that each 100-ps pulse produces the same amount of internal lasing radiation. If the intensity ratio of radiation that leaked from the Descartes ring (peak 2) and the rim (peak 1 or 3) had remained independent of the number of 100-ps pulses, then we would be forced to conclude that the light leakage rate from the Descartes ring is also independent of the occurrence of previous pulses; i.e., the perturbation at the Descartes ring results from a quasi-instantaneous mechanism [such as $\Delta m(\omega, I_{in}) = n_2 I_{in}(t)$] and not a cumulative mechanism (such as electrostriction or thermal effects). However, what we observed is that the intensity ratio of peak 2 and peak 1 increases with the number of 100-ps pulses. Therefore from the multiple 100-ps laser pulse result we conclude that the perturbation mechanism at the Descartes ring can also have a cumulative component, because the leakage rate increases with the number of 100-ps pulses that are incident on the droplet.

From the single-pulse result for ethanol droplets we observe that the quasi-instantaneous effects cause some extra laser light leakage through the high-surface-intensity regions (Descartes ring). Although cumulative thermal perturbation may also cause the extra leakage, results shown below suggest that the thermal perturbation may not be so important as numerical estimations indicate. However, from multiple-pulse results we observe that the extra leakage is enhanced as a result of cumulative perturbation mechanisms that could be electrostrictive surface bulging at the Descartes ring and/or bulging caused by surface tension lowering because of temperature rise. For multiple-pulse irradiation we conclude that cumulative as well as quasi-instantaneous perturbations lead to extra leakage of the lasing radiation. Although the estimate of $\Delta m(\omega, T)$ shows that temperature effect is more prominent than the $\Delta m(\omega, I)$, from our experimental results with multiple pulses we could not distinguish these two temperature effects.

One or More 100-ps Pulses: CS_2–Ethanol Mixture Droplets

Figure 10(a) shows the CCD-captured image of a lasing CS_2–ethanol droplet ($a = 25.5$ μm) irradiated with five consecutive 100-ps pulses. Figure 10(b) shows the digitized intensity distribution of the CCD image displayed in Fig. 10(a). The blurred spot within the droplet rim [shown in Fig. 10(a)] is much more intense than the radiation from the droplet rim. Consequently, in Fig. 10(a), in order to display the relatively weak intensity emerging from the rim we increased the rim intensity scale by 8× relative to the intensity scale for other portions of the droplet image. Instead of observing a crescent shape image at the Descartes ring [e.g., as in the case for ethanol droplets; see Fig. 7(a)], we observed a blurred spot that has some fine structures [see Track A of Figs. 10(a) and 10(b) for CS_2–ethanol droplets]. The fine structure of the blurred spot, which is imaged along Track A, consists of two intensity peaks labeled 5 and 6 in Fig. 10(b).

Figure 10(c) presents the top view of droplet equatorial plane and the expected image along the CCD Track A. Intensity peaks 1 and 3 correspond to the projection of the radiation leakage from the droplet rim onto the CCD Track A [similar to Fig. 7(c)]. From the theoretical computation of the internal and surface intensity [see Fig. 3(a)], we can predict what is expected to be observed. Intensity peak 6 corresponds to the location of the largest surface intensity maximum that is along the droplet principal axis $\phi = 0°$ and not from the smaller surface intensity maximum at the Descartes ring [$\phi_D = 8.6°$; see Fig. 3(b)]. Because the collection optics magnifies the droplet, we are able to distinguish between light emerging from the Descartes ring on the droplet surface (at an observation angle $\phi_{obs} = 38° + 8.6°$) and from a surface spot along the principal axis (at $\phi_{obs} = 38° + 0°$), correspond-

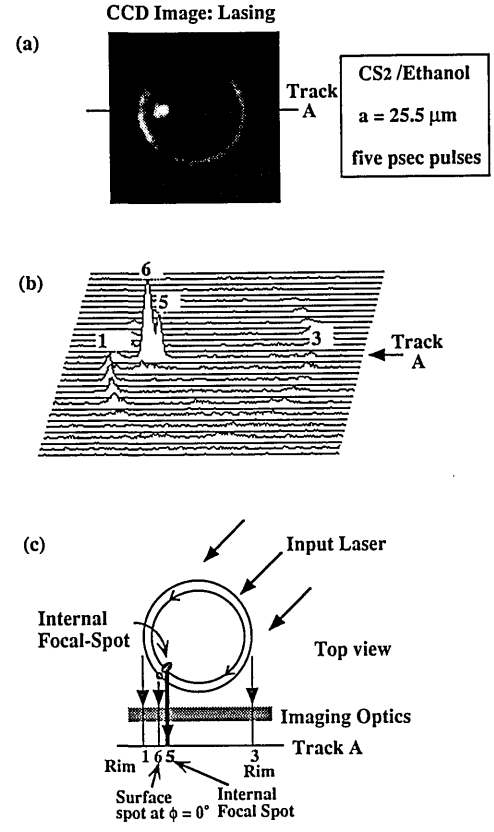

Fig. 10. (a) Gray-scale image from the CCD camera of a CS_2–ethanol (80% CS_2 and 20% ethanol) droplet containing 2×10^{-4} M Rhodamine 6G irradiated by five consecutive 100-ps green ($\lambda_{input} = 532$ μm) pulses within a single Q-switched burst. (b) The digitized CCD image shown in (a). (c) An illustration of the specific regions on the droplet equatorial plane where the leakage radiation is detected along CCD Track A.

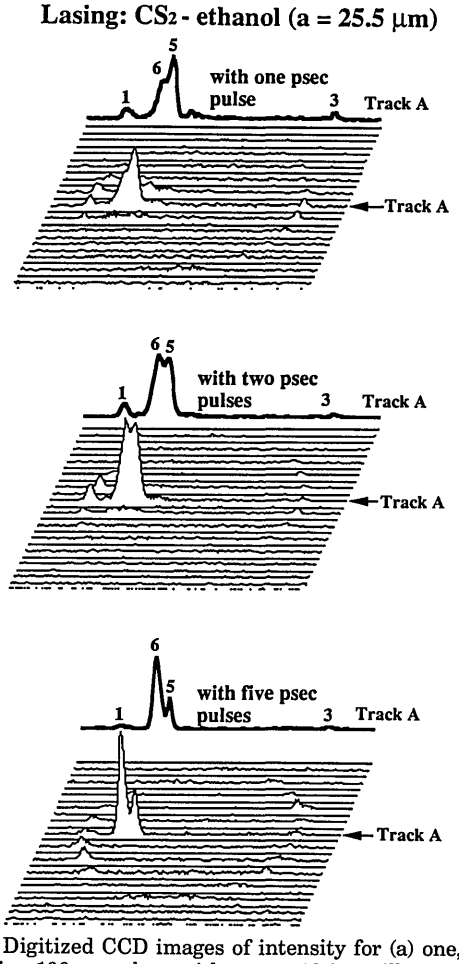

Fig. 11. Digitized CCD images of intensity for (a) one, (b) two, and (c) five 100-ps pulses with $t_{p-p} = 13.2$ ns illuminating the CS_2–ethanol droplets containing 2×10^{-4} M Rhodamine 6G. On top of each digitized plot the CCD Track A content is plotted (corresponding to the droplet equatorial plane shown in Fig. 10) with a thick line. Intensity peaks 1 and 3 are the normal MDR leakage from the droplet rim, and intensity peak 6 is the extra leakage from the surface bulge at $\phi = 0°$. In these plots, intensity peak 5 is from the interior high-intensity region between the front-focal spot and the shadow surface [see Fig. 3(c)].

ing to peak 6. If the radiation leakage had originated from the Descartes ring at $\phi_D = 8.6°$, the spatial position of intensity peak 6 would have to appear closer to intensity peak 1. Intensity peak 5 corresponds to dye-lasing radiation emerging from the internal front-focal region just within the droplet surface. However, the spatial distribution in the front-focal region appears distorted on leaving the spherical liquid–air interface.

For one, two, and five 100-ps pulses, Fig. 11 shows the digitized images as well as the intensity distribution along the CCD Track A, which is plotted as a thick line. Unlike that of the gray-scale CCD images shown in Fig. 10(a), the intensity scale of the digitized images [shown in Figs. 10(b) and 11] is the same throughout each plot. The radiation leakage on the droplet surface at $\phi = 0°$ (peak 6) and from the droplet interior front-focal spot (peak 5) is much greater than the MDR-related leakage from the rim (peaks 1 and 3). Note that in Fig. 11 the intensity ratio of peak 6 and peak 5 increases as the number of consecutive 100-ps pulses increases.

The observation that the leakage from the surface at $\phi = 0°$ and the front-focal spot region of CS_2–ethanol droplet is larger than from its rim and the surface at $\phi_D = 18.6°$ of ethanol droplets may be attributed to the following causes. First, because of the increased $m(\omega)$ for CS_2–ethanol droplets, the internal intensity maximum of the front-focal spot region is closer to the droplet shadow surface and has a better spatial overlap with the dye-lasing fields, which are on high Q MDR's. Second, an increase of $m(\omega)$ causes the surface intensity maximum to shift to $\phi = 0°$ and to have a larger intensity enhancement. Correspondingly, $\Delta m(\omega, I_{in})$ and $\Delta m(\omega, \Delta T)$ are larger at the CS_2–ethanol surface at $\phi = 0°$ and near the front-focal spot region. Third, n_2 for the CS_2–ethanol droplets is an order of magnitude larger than that for ethanol droplets. The combined effects of better spatial overlap of the large internal intensity region with the MDR's supporting lasing radiation, larger intensity enhancement on the surface and in the interior, and larger n_2 cause more $\Delta m(\omega)$-related elastic scattering.

The scattered image from the internal high-intensity region of CS_2–ethanol droplets will appear distorted by the spherical droplet–air interface. The $\Delta m(\omega, I_{in})$-related elastic scattering at the front-focal spot of CS_2–ethanol droplets is independent of the surface bulge, and thus the measured intensity of peak 5 should not be dependent on the persistent nature of the surface bulge. Figures 10 and 11 show that the intensity ratio of peak 5 (from the front-focal spot region) and peak 1 or peak 3 (from the rim) remains fairly constant as the number of input-laser pulses is increased. We conclude that the dye-laser radiation emerging from the front-focal spot region is caused by a quasi-instantaneous perturbation.

The manifestations of the laser-induced surface perturbations at $\phi = 0°$ of CS_2–ethanol droplets is quite different. As the surface bulge grows in time, the MDR-supported dye-laser radiation encounters more surface perturbations normal to its propagation direction. Consequently, the leakage rate of the dye-laser radiation increases as the surface bulge amplitude develops. In Fig. 11 the intensity ratio of peak 6 (from the surface at $\phi = 0°$) and peak 5 (from the front-focal spot region) increases with the number of 100-ps pulses. From the intensity ratios of peak 6 and peak 5 with an increasing number of 100-ps pulses, we conclude that peak 6 is the leakage caused by a cumulative mechanism, such as a surface bulge induced by electrostriction and/or by thermal reduction of surface tension.

Because the laser dye is absorbing ($\alpha \approx 7$ cm^{-1}), a temperature rise at the high-intensity regions could cause cumulative perturbations. The estimated temperature rise at the surface maxima of the intensity is 13°C and at the front-focal spot is 25°C per 100-ps pulse. The temperature rise at the surface could lower the surface tension and thereby cause a surface bulge. A temperature rise at or near the front-focal spot may also cause $\Delta m(\omega, \Delta T)$ and, thereby, some extra scattering from that internal region. All these thermal effects are cumulative. However, the fact that the intensity ratio of peak 5 (from the internal focal spot) and of peak 1 or peak 3 (from the rim) is nearly independent of number of 100-ps pulses implies that $\Delta m(\omega, \Delta T)$ is not significant. From the experimental data related to intensity peak 6 (from the surface at $\phi = 0°$), it is not possible to isolate the thermal perturbation from the electrostrictive or $\Delta m(\omega, I_{in})$ perturbation.

For ethanol droplets the elastic scattering of the dye-laser radiation at the front-focal spot is not detected by the CCD for several possible reasons. First, compared with CS_2–ethanol droplets, $\Delta m(\omega, I_{in})$ is smaller because n_2 of ethanol is lower and the intensity enhancement at the front-focal point is also lower. Second, compared with CS_2–ethanol droplets, the high-intensity enhancement region around the front-focal spot of ethanol droplets is more localized and situated farther away from the droplet surface [see Fig. 1(b)]. Consequently, the spatial overlap between the perturbed region of $\Delta m(\omega)$ and the MDR-supported dye-laser field is also less, thereby leading to less $\Delta m(\omega)$-related elastic scattering.

The experimental result for CS_2–ethanol droplets irradiated with a single 100-ps pulse shows that the quasi-instantaneous perturbation $\Delta m(\omega, I_{in})$ causes extra-light leakage from the surface high-intensity region as well as the front-focal spot region. The cumulative effect of electrostrictive bulge and/or thermally induced bulge resulting from surface tension lowering is evident in the multiple-pulse result. The quasi-instantaneous nature of the leakage from the front-focal spot region indicates that the thermally induced refractive-index change is not important, which is contrary to our estimates of $\Delta m(\omega, \Delta T)$.

Lasing in D_2O Droplets Irradiated with Green and Near-IR Beams

The main motivation for this phase of our experiment is to attempt to isolate laser-induced perturbations associated with inhomogeneous heating. We use a Q-switched Nd:YAG laser to provide two simultaneously emitting laser beams, one in the green (beam A with $\lambda_A = 0.532$ μm) and the other in the near IR (beam B with $\lambda_B = 1.064$ μm). The angle between these two laser beams is adjusted to be 90°. Figure 12(a) shows that the angle between the observation direction and the propagation direction of beam A is ϕ_A and that of beam B is ϕ_B. The collection optics is set for $\phi_A = \phi_B = 45°$. The two incident laser beams ought to produce two Descartes rings, ring A and ring B [see Fig. 12(a)]. Rays 1 and 3, which are both tangent to the droplet rim, are the normal leakage of MDR's from an unperturbed droplet. Rays 2A and 2B are the extra leakage from the laser-induced perturbation from the droplet surface. Because of axial symmetry, rays 1 and 3 appear as a ring and rays 2A and 2B appear as two opposite facing crescents.

The two laser beams are adjusted to have $I_A = I_B = 0.24$ GW/cm^2 and have nearly the same pulse duration of $\approx$7 ns. For Rhodamine 6G at a concentration of 1×10^{-5} M in D_2O, the measured absorption coefficient is $\alpha_A = 0.7$ cm^{-1} in the green and $\alpha_B \approx 0$ cm^{-1} in the near IR. Thus, when the two beams have equal irradiance and fluence, there should be a surface and volume temperature rise induced by the green beam A (i.e., $\Delta T_A > 0°$) and nearly no surface and volume temperature rise induced by the near-IR beam B (i.e., $\Delta T_B \approx 0°$). Consequently, if temperature-related perturbation mechanisms are important and if all the other perturbative mechanisms are equal for beams A and B, then the dye-laser radiation leakage from Descartes ring A ought to be brighter than that from Descartes ring B. By comparing the relative intensity of the red-dye-lasing radiation leakage from Descartes ring A and from Descartes ring B, we anticipate that it may be possible to isolate the surface temperature-rise-related perturbations. These thermal perturbations involve $\Delta m(\omega, \Delta T)$ on the droplet surface and near the front-focal spot region and also involve a surface bulge because of the lowering of the surface tension localized at the high-surface-intensity region.

Figure 12(b) is the CCD image (in gray scale) of a D_2O droplet containing 1×10^{-5} M Rhodamine 6G. The droplet image consists of two oppositely facing red Descartes crescents created by the green laser beam A and the near-IR-laser beam B. The different appearance of the two Descartes crescents is attributed to the poor beam quality of the near-IR laser output, which is inadvertently more inhomogeneous than the spatial distribution of the green beam. Because the near-IR beam is not visible, it is more difficult to select a smooth portion of the near-IR beam with a spatial filter, as is done for the green laser beam.

From the CCD image shown in Fig. 12(b) we noted that the brightness of Descartes rings A and B is comparable, even though we estimated $\Delta T_A \approx 7°$C and $\Delta T_B \approx 0°$C on the droplet surface of the Descartes ring. This surprising result indicates that the laser-induced surface heating did not produce a perceptible amount of additional leakage at the Descartes ring A. Our observation with two 7-ns-duration beams, where the green beam is absorbed and the near-IR beam is not absorbed, suggests that the perturbations induced by slightly heated and nonheated surfaces at the Descartes rings are nearly equal. Even though the temperature rise perturbations could not be

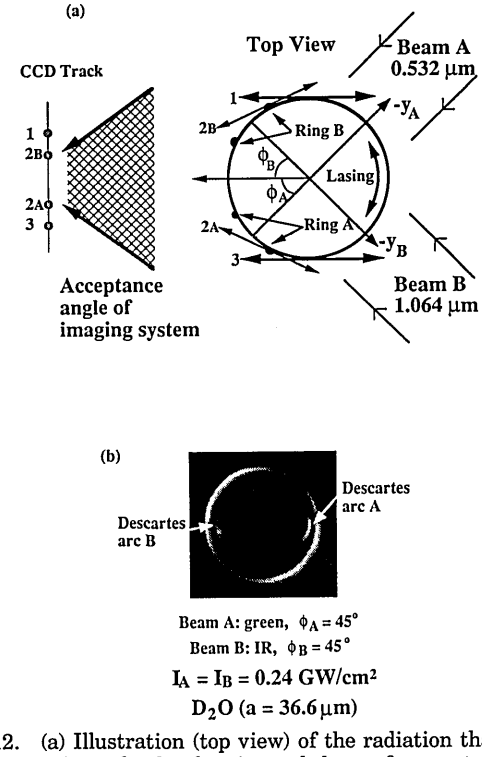

Fig. 12. (a) Illustration (top view) of the radiation that tangentially leaks from the droplet rim and the surface perturbation at the Descartes ring. The D_2O droplet ($a = 25.2$ μm) is irradiated with a green beam A ($\lambda_A = 0.532$ μm) and a near-IR beam B ($\lambda_B = 1.064$ μm) at 90° to each other. The duration of each beam is 7 ns. The observation angles relative to the two beam directions are $\phi_A = \phi_B = 45°$. (b) The gray-scale image from the CCD camera of a 1×10^{-5} M Rhodamine 6G D_2O droplet irradiated by a green beam and a near-IR beam.

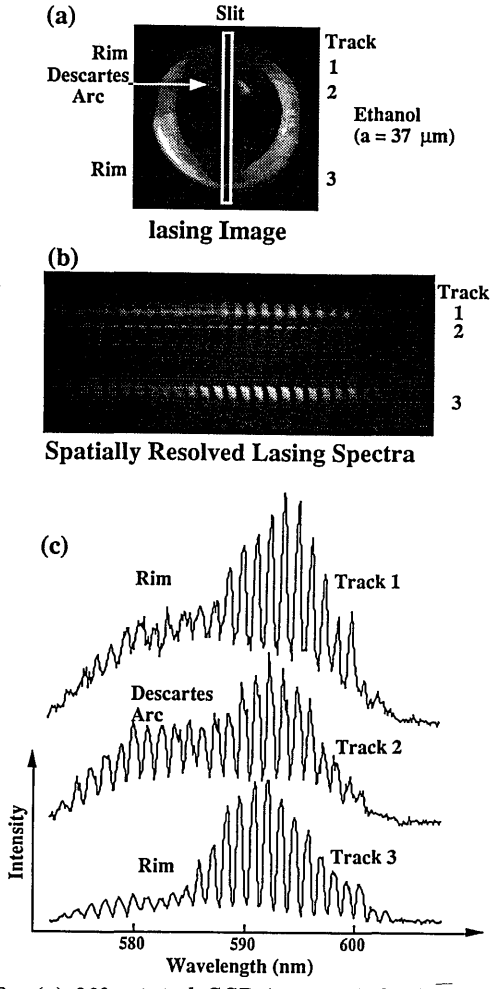

Fig. 13. (a) 90°-rotated CCD image of the lasing droplet ($a = 37$ μm) irradiated with a frequency-doubled 7-ns Nd:YAG Q-switched laser pulse ($\lambda_{input} = 0.532$ μm). The spectrograph slit collects leakage radiation from the two opposite segments of the rim and the Descartes arc. The locations are shown for CCD Tracks 1, 2, and 3. (b) The gray-scale image of spatially resolved spectra dispersed by a spectrograph. (c) The intensity from CCD Tracks 1, 2, and 3 [shown in the gray-scale image of (b)] as a function of the wavelength. Tracks 1 and 3 correspond to the light coming from the rim, and track 2 corresponds to the light coming from the Descartes arc.

isolated from other perturbations, such as from $\Delta m(\omega, I_{in})$ and the pure electrostrictive effect, the temperature-related perturbations on the droplet surface are not that significant in comparison with the other perturbation mechanisms. We further infer that the perturbations caused by temperature rise by the single and multiple 100-ps pulses must also not be important, since the ΔT rise with these low-fluence pulses irradiating 2×10^{-4} M Rhodamine 6G ethanol and CS_2–ethanol droplets is even lower than the temperature rise caused by the 7-ns pulse.

Lasing Spectrum: Simultaneous Measurement

When an aperture is used in the collection optics, the separately detected SRS spectra from the Descartes ring and the droplet rim are found to be the same, both exhibiting the same MDR-related peaks.[9] As an affirmation of this previous finding,[9] we elected spatial resolution of the lasing spectra from various regions of a laser-dye-doped ethanol droplet ($a \approx 37$ μm), which is pumped by a single green laser beam. With one input laser firing (with the second harmonic of a Q-switched Nd:YAG laser of 7-ns duration), we are able to detect simultaneously the red laser radiation leakage from a portion of the Descartes crescent and from a portion of the two diametrically opposite segments of the droplet rim.

A dove prism is used to rotate the droplet image by 90° about the viewing axis. Consequently, the vertical spectrograph slit encompasses a portion of the Descartes crescent and the two opposite segments of the droplet rim in the original equatorial plane [see Fig. 13(a)]. In order to increase the spatial separation of the Descartes ring from the rim, the measurement is made with the observation angle set at $\phi_{obs} = 20°$ and the collection optics focused on the Descartes arc and thereby out of focus for the droplet rim. By placing the CCD at the exit plane of a spectrograph we are able to measure the spectrograph-dispersed spectra along the CCD horizontal tracks while preserving the spatial image of the spectrograph slit along the CCD vertical tracks.

The gray-scale output of the CCD detector is displayed in Fig. 13(b). The vertical tracks of the CCD output correspond to the droplet image along the vertical spectrograph slit [shown in Fig. 13(a)], and the horizontal tracks of the CCD output correspond to the dispersed spectra of the dye-lasing radiation. Note that the two out-of-focus rim segments span many more vertical CCD tracks, while the in-focus Descartes crescent or arc spans only a few vertical CCD tracks. The CCD Track 1 is situated within the top portion of the out-of-focus droplet rim, Track 2 is situated within a portion of in-focus Descartes arc, and Track 3 is situated within the bottom portion of the out-of-focus droplet rim. Figure 13(c) displays the signals in Tracks 1, 2, and 3. There exists a remarkable spectral correlation among the numerous MDR-related lasing peaks that are all within the Rhodamine 6G gain profile. Similar spectral correlation is found if the droplet image is slightly displaced more to the left or right relative to the vertical spectrograph slit [see Fig. 13(a)]. We conclude with a high degree of certainty that the red-lasing radiation emerging from any portion of the droplet rim and the Descartes arc is associated with the same set or sets of MDR's.

CONCLUSIONS

We have attempted to isolate various laser-induced perturbation mechanisms that cause extra leakage of the internally generated dye-laser radiation. The experimental results demonstrate that besides quasi-instantaneous perturbations there are cumulative perturbations, which persist and even develop after each input-laser pulse is over. These quasi-instantaneous and cumulative perturbations confirm the conjectures and experimental evidences by others.[9–13] By monitoring the leakage of dye-laser radiation and not the SRS, we avoided working near the LIB threshold and thus avoided generating plasmas and all the plasma-related light absorbing and scattering complications. Possible perturbations associated with short and long lifetime acoustic phonons generated by intense SBS is ruled out because the optical absorption of Rhodamine 6G degrades the droplet cavity Q in the green and suppresses SBS. However, because of the absorption at the incident

laser frequency, temperature-related perturbations are introduced. Consequently, $\Delta m(\omega, \Delta T)$ is not readily separable from $\Delta m(\omega, I_{in})$. In addition, temperature-rise-induced surface tension lowering is not readily separable from pure electrostriction-induced surface bulge.

The experimental results with ethanol droplets containing Rhodamine 6G lead us to conclude that there exist cumulative mechanisms acting on the surface at the Descartes ring along with some quasi-instantaneous perturbations. For CS_2–ethanol droplets the nearly constant intensity ratio of the leakage from the front-focal spot region and from the droplet rim, with increasing numbers of 100-ps pulses, indicates that the extra leakage from the front-focal point region is ascribed to elastic scattering associated with a $\Delta m(\omega)$ resulting from $n_2 I_{in}$ and not from $(\partial n/\partial T)\Delta T$. This experimental observation is contrary to our numerical estimates, which indicate that at the front-focal spot, $\Delta m(\omega, \Delta T)$ is an order of magnitude higher than $\Delta m(\omega, I_{in})$. Furthermore, for CS_2–ethanol droplets the observation of the growing intensity ratio of the leakage from the surface at $\phi = 0°$ and the droplet rim, with increasing numbers of 100-ps pulses, suggests that there is a cumulative component to the surface perturbation. However, we are unable to isolate the pure electrostrictive mechanism from the two temperature-related perturbations, surface tension lowering and $\Delta m(\omega, \Delta T)$. The temperature-related mechanism is investigated in specific with two different-wavelength laser pulses with high fluence. Again, the temperature-related perturbations are found experimentally not to be dominant compared with the $\Delta m(\omega, I_{in})$ perturbation, contrary to our estimates of $\Delta m(\omega, \Delta T)$ and $\Delta m(\omega, I_{in})$ at various high-intensity regions. We are not able to conclude whether temperature-related surface bulge is important, as we were unable to estimate accurately the surface bulge amplitude associated with surface tension lowering because of an inhomogeneous temperature rise.

With only two coincident approximately 7-ns pulses of different wavelengths, we are not able to emphasize the relative importance of the quasi-instantaneous $\Delta m(\omega, I_{in})$ and of the cumulative electrostrictive bulge. On the basis of the results of other researchers with two time-delayed laser pulses[9] and our present results with multiple 100-ps laser pulses, the electrostrictive bulge contribution can be made evident as the observation time is increased, and thus the bulge is allowed to develop after each pulse and accumulates the fluences of all the laser pulses. In our opinion, continued study of laser-induced perturbations in the droplet interior and on the droplet surface is warranted, because both the MDR feedback and the cavity-QED gain enhancement factor are dependent on the overall Q of the droplet cavity.

ACKNOWLEDGMENTS

We gratefully acknowledge the partial support of this research by the U.S. Army Research Office (contract DAAL03-91-G-0042 at Yale University and contract DAAL03-90-G-0143 at Clarkson University). We acknowledge many helpful discussions with Kenneth Young at the Chinese University of Hong Kong.

REFERENCES

1. S. C. Hill and R. E. Benner, "Morphology-dependent resonances," in *Optical Effects Associated with Small Particles*, P. W. Barber and R. K. Chang, eds. (World Scientific, Singapore, 1988), p. 3.
2. H.-M. Tzeng, K. G. Wall, M. B. Long, and R. K. Chang, "Laser emission from individual droplets at wavelengths corresponding to morphology-dependent resonances," Opt. Lett. **9,** 499 (1984); S.-X. Qian, J. B. Snow, H.-M. Tzeng, and R. K. Chang, "Lasing droplets: highlighting the liquid–air interface by laser emission," Science **231,** 486 (1986); H.-B. Lin, A. L. Huston, B. J. Justus, and A. J. Campillo, "Some characteristics of a droplet whispering-gallery-mode laser," Opt. Lett. **11,** 614 (1986).
3. J. B. Snow, S.-X. Qian, and R. K. Chang, "Stimulated Raman scattering from individual water and ethanol droplets at morphology-dependent resonances," Opt. Lett. **10,** 37 (1985); H.-B. Lin, A. L. Huston, J. D. Eversole, and A. J. Campillo, "Double-resonance stimulated Raman scattering in micrometer-sized droplets," J. Opt. Soc. Am. B **7,** 2079 (1990); A. Biswas, H. Latifi, R. L. Armstrong, and R. G. Pinnick, "Double-resonance stimulated Raman scattering from optically levitated glycerol droplets," Phys. Rev. A **40,** 7413 (1989).
4. J.-Z. Zhang and R. K. Chang, "Generation and suppression of stimulated Brillouin scattering in single liquid droplets," J. Opt. Soc. Am. B **6,** 151 (1989); F. H. Wirth, K. A. Juvan, D. H. Leach, J. C. Swindal, R. K. Chang, and P. T. Leung, "Phonon-retention effects on stimulated Brillouin scattering from micrometer-sized droplets illuminated with multiple short laser pulses," Opt. Lett. **17,** 1334 (1992).
5. J.-Z. Zhang, D. H. Leach, and R. K. Chang, "Photon lifetime within a droplet: temporal determination of elastic and stimulated Raman scattering," Opt. Lett. **13,** 270 (1988).
6. H. M. Lai, P. T. Leung, and K. Young, "Limitations on the photon storage lifetime in electromagnetic resonances of highly transparent microdroplets," Phys. Rev. A **41,** 5199 (1990).
7. A. L. Huston, H.-B. Lin, J. D. Eversole, and A. J. Campillo, "Effect of nanometer bubble formation on microdroplet cavity quality factor," from A. J. Campillo, Naval Research Laboratory, Washington, D.C. 20375 (personal communication).
8. M. A. Jarzembski and V. Srivastava, "Electromagnetic field enhancement in small liquid droplets using geometric optics," Appl. Opt. **28,** 4962 (1989).
9. J.-G. Xie, T. E. Ruekgauer, J. Gu, R. L. Armstrong, and R. G. Pinnick, "Observations of Descartes ring stimulated Raman scattering in micrometer-sized water droplets," Opt. Lett. **16,** 1310 (1991).
10. J.-G. Xie, T. E. Ruekgauer, J. Gu, R. L. Armstrong, R. G. Pinnick, and J. D. Pendleton, "Physical basis for Descartes ring scattering in laser-irradiated microdroplets," Opt. Lett. **16,** 1817 (1991).
11. R. G. Pinnick, G. A. Fernández, J.-G. Xie, T. Ruekgauer, J. Gu, and R. L. Armstrong, "Stimulated Raman scattering and lasing in micrometer-sized cylindrical liquid jets: time and spectral dependence," J. Opt. Soc. Am. B **9,** 865 (1992).
12. V. Srivastava and M. A. Jarzembski, "Laser-induced stimulated Raman scattering in the forward direction of a droplet: comparison of Mie theory with geometrical optics," Opt. Lett. **16,** 126 (1991).
13. J.-Z. Zhang and R. K. Chang, "Shape distortion of a single water droplet by laser-induced electrostriction," Opt. Lett. **13,** 916 (1988).
14. H. M. Lai, P. T. Leung, K. L. Poon, and K. Young, "Electrostrictive distortion of a micrometer-sized droplet by a laser pulse," J. Opt. Soc. Am. B **6,** 2430 (1989).
15. F. H. Wirth, K. A. Juvan, D. H. Leach, J. C. Swindal, R. K. Chang, and P. T. Leung, "Phonon-retention effects on stimulated Brillouin scattering from micrometer-sized droplets illuminated with multiple-short laser pulses," Opt. Lett. **17,** 1334 (1992).